

See discussions, stats, and author profiles for this publication at: <https://www.researchgate.net/publication/245032817>

# Hyperspectral Imaging and Chemometrics: A Perfect Combination for the Analysis of Food Structure, Composition and Quality

Chapter · July 2013

CITATIONS

25

READS

2,084

3 authors:



José Manuel Amigo

Universidad del País Vasco / Euskal Herriko Unibertsitatea

149 PUBLICATIONS 2,243 CITATIONS

[SEE PROFILE](#)



Idoia Martí-Aluja

7 PUBLICATIONS 54 CITATIONS

[SEE PROFILE](#)



Aoife Gowen

University College Dublin

121 PUBLICATIONS 2,426 CITATIONS

[SEE PROFILE](#)

Some of the authors of this publication are also working on these related projects:

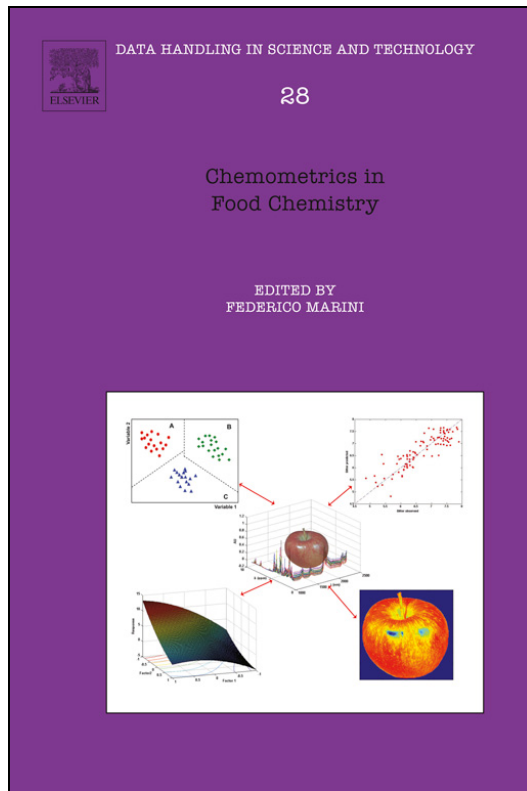
Project

Campydecon: Controlling Campylobacter Contamination in Poultry Processing [View project](#)

Project

Investigation on milk foam quality for use in espresso based milk drinks [View project](#)

This chapter was originally published in the book *Data Handling in Science and Technology*, Vol. 28, published by Elsevier, and the attached copy is provided by Elsevier for the author's benefit and for the benefit of the author's institution, for non-commercial research and educational use including without limitation use in instruction at your institution, sending it to specific colleagues who know you, and providing a copy to your institution's administrator.



All other uses, reproduction and distribution, including without limitation commercial reprints, selling or licensing copies or access, or posting on open internet sites, your personal or institution's website or repository, are prohibited. For exceptions, permission may be sought for such use through Elsevier's permissions site at:

<http://www.elsevier.com/locate/permissionusematerial>

From: José Manuel Amigo, Idoia Martí and Aoife Gowen, Hyperspectral Imaging and Chemometrics: A Perfect Combination for the Analysis of Food Structure, Composition and Quality. In Federico Marini, editor: Data Handling in Science and Technology, Vol. 28, Amsterdam: The Netherlands, 2013, pp. 343-370.  
ISBN: 978-0-444-59528-7  
© Copyright 2013 Elsevier BV.  
Elsevier

## Chapter 9

# Hyperspectral Imaging and Chemometrics: A Perfect Combination for the Analysis of Food Structure, Composition and Quality

José Manuel Amigo<sup>\*1</sup>, Idoia Martí<sup>†</sup> and Aoife Gowen<sup>‡</sup>

<sup>\*</sup>Department of Food Science, Quality and Technology, Faculty of Life Sciences, University of Copenhagen, Frederiksberg C, Denmark

<sup>†</sup>Analytical and Organic Chemistry Department, Universitat Rovira i Virgili, Tarragona, Spain

<sup>‡</sup>School of Biosystems Engineering, University College Dublin, Dublin 4, Ireland

<sup>1</sup>Corresponding author: jmar@life.ku.dk

## Chapter Outline

<b>1. Introduction</b>	<b>344</b>	3.1 Overview of HSI Data Analysis	352
1.1 Quality Assessment	344	3.2 Pre-processing Methods	353
1.2 The Role of Hyperspectral Image in Food Quality Assessment	345	3.3 Unsupervised Techniques to Explore the Image: PCA	355
1.3 The Need for Chemometrics	345	3.4 Supervised Techniques for Classification of Features	358
1.4 Objective of the Book Chapter	350	3.5 Regression Modelling for Obtaining Quantitative Information from Hyperspectral Images	362
<b>2. Structure of a Hyperspectral Image</b>	<b>350</b>	<b>4. Final Remarks</b>	<b>364</b>
<b>3. Hyperspectral Analysis and Chemometrics: Practical Examples</b>	<b>352</b>	<b>References</b>	<b>366</b>

## 1 INTRODUCTION

### 1.1 Quality Assessment

Defining quality in food production is, arguably, one of the most widespread and complicated issues to solve when new products are released in the market. In short, food quality can be defined as the characteristics of food that are between certain limits of acceptance in every step of manufacturing, from the raw materials to the acceptance of consumers (Figure 1). This makes the definition of quality even more cumbersome, since each product will have its own requirements of quality in every step of the production chain. For instance, equally important are external factors (e.g. gloss, colour, packaging conditions), sensory parameters (e.g. texture, flavour), certificates of origin, process variables (e.g. grain size, ageing, fermentation parameters) and product traceability in the final quality definition. Therefore, quality assessment of the final product depends directly on the assessment of quality at every step of the food processing chain.

Quality control at every step of the manufacturing chain must be adapted to the needs of a growing market where products must be manufactured in a fast and robust manner. The concept of global quality control by assessing quality at every step of the production chain was introduced by the U.S. Food and Drug Administration (FDA), which launched the process analytical technology (PAT) initiative to transform approaches to quality assurance in every step of the process [1]. This initiative encourages the implementation of three basic ideas [2]:

1. Real-time process analyzers and control tools.
2. New multivariate tools for experimental design and data analysis.
3. Utilization of (1) and (2) for continuous improvement and knowledge of the process.

Decisions must be taken in a real-time framework to ensure product quality, safety, authenticity, and compliance with labelling [3]. Traditional analytical methods involving techniques such as high performance liquid chromatography (HPLC) are expensive, time-consuming, do not offer a real-time feedback

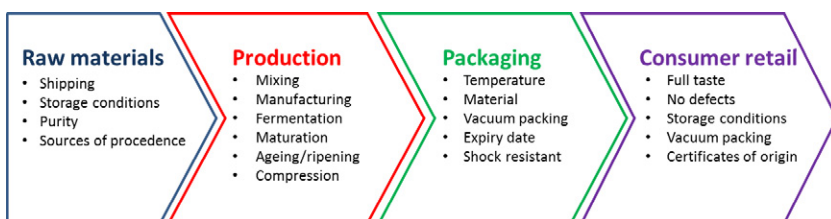


**FIGURE 1** General scheme and examples of controlling variables in a food processing chain.

about the evolution of the processes, and typically require destruction of the sample. However, these techniques usually offer a comprehensive understanding of the physicochemical parameters affecting a particular process. An example of this is the process of apple ripening, which can be studied by Gas chromatography–mass spectrometry (GC–MS) to obtain a complete view of the evolution of the constituents during the ripening process [4]. However, using this technique it is not possible to give a fast and reliable response about the adequacy of the apple for the market. This problem can be solved with the implementation of sensors that do not measure specific constituents of the apples, but relate ripening to an easy-to-measure property like colour [5]. By doing this, a fast and real-time response can be given about the point at which an apple is adequate for the market.

The framework of total quality control in a fast and reliable manner has driven the application of machine vision devices within the food industry in recent years. Digital colour systems (e.g. Red–Green–Blue (RGB) systems) now find widespread use in food quality control for the detection, for instance, of surface defects and grading operations [6]. Nevertheless, the information that can be obtained from a colour camera is limited to the vision range of the three colour channels. To overcome this problem, multichannel imaging and, especially, hyperspectral imaging systems have been adapted to laboratory or line production scale to gather a huge amount of spectral information of one surface in a relative short time.

## 1.2 The Role of Hyperspectral Image in Food Quality Assessment

Hyperspectral imaging extends the capability of traditional imaging techniques by obtaining spatial images of a sample at a series of ( $>100$ ) contiguous wavelengths. Thus, each pixel of a hyperspectral image can be interpreted as a spectrum (Figure 2). This technique has recently emerged as a process analytical tool for food quality assessment, offering an immense amount of spectral and spatial information from a sample. The attractiveness of attaining both spatial and spectral information from an object (Figure 2) is that it provides reliable and accurate information at different stages of the food processing chain. Proof of the latter is confirmed by the wide range of applications found in the literature [3,7–13].

## 1.3 The Need for Chemometrics

The main difference of a hyperspectral image with respect to other imaging techniques is that for each pixel, a whole spectrum is obtained. The resulting large quantity of data is not exempt of issues, as pointed out by Amigo in the framework of pharmaceutical preparations [14]. The main issue is extracting useful and meaningful information from the raw images. Chemometrics is

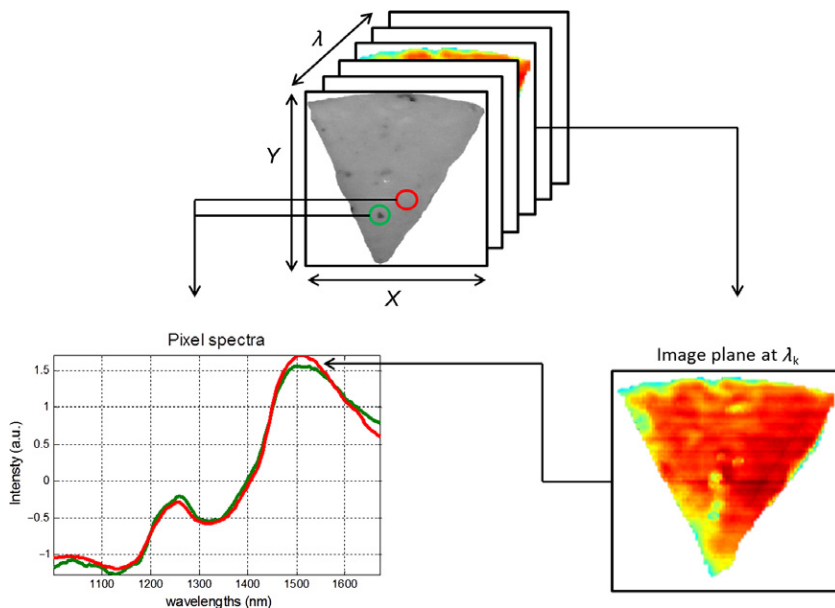


**FIGURE 2** Schematic representation of a near infrared (NIR) hyperspectral image of cheese showing the relationship between spectral ( $\lambda$ ) and spatial ( $X$ - $Y$ ) dimension.

an appealing tool for this task because it allows us to: reduce the dimensionality of the data; retain essential spectral information and classify or quantify important areas of a scene [3,15]. Chemometric methods can be grouped according to the information desired from their application, as follows [2,3,15]:

- *Qualitative/exploratory analysis*: for example principal component analysis (PCA), fixed size image window–evolving factor analysis (FSIW–EFA).
- *Supervised and unsupervised classification*: for example PCA, K-means and fuzzy clustering, linear discriminant analysis (LDA), partial least squares-discriminant analysis (PLS-DA), fisher discriminant analysis (FDA), artificial neural networks (ANN).
- *Resolution and quantization*: for example multivariate curve resolution (MCR), partial least squares regression (PLSR), ANN for regression, multi-linear regression (MLR), and classical least squares (CLS).

There have been many applications of chemometrics and HSI to foodstuffs for different purposes. They can be divided into four main groups: Fruits and vegetables, meat, dairy products, and grains. In each group the needs are different, as can be appreciated in Table 1. For instance, the main applications in fruits, vegetables and meat are to find external defects/properties; whereas sorting is one of the main applications in grains. Table 1 shows a comprehensive view of the main applications in the four groups mentioned.

**TABLE 1** Main Applications of HIS and Chemometrics in Foodstuff

Sample	Application	Analytical technique	Chemometrics technique	Reference
Apples	Detection of bruises	Vis-NIR HSI	PCA, ANN, MLR	[16]
	Detection of bitter pit defects	NIR HSI	PLS	[16]
	Prediction of the firmness and soluble solids content	Vis-NIR HSI	ANN, MLR	[17,18]
	Detection of chilling injury	Vis-NIR HSI	ANN	[17]
	Detection of physical properties	Vis-NIR HSI	PCA	[19]
	Detection of defects on the surface	UV-vis-NIR HSI	ANN	[20]
	Quantization of starch distribution	Vis-NIR HSI	PLS	[21,22]
	Quantization of starch content	NIR HSI	PLS-DA	[23]
	Ripening	Vis-NIR HSI	PLS-DA	[5]
	Quantization of sugar content	NIR HSI	PLS	[22]
Cucumbers	Detection of chilling injury	Vis-NIR HSI	PCA, FLD (k-NN)	[24,25]
	Detection of internal defects	Vis-NIR HSI	PLS-DA	[26]
	Detection of defects on the surface	Vis-NIR HSI	PCA	[27]
Citrus	Detection of skin defects	RGB and NIR HSI, fluorescence imaging	LDA	[28]
	Detection of rottenness caused by bacteria	Vis-NIR HSI	LDA	[29]
	Detection of bruises	Vis-NIR HSI	PCA	[30]

*Continued*

**TABLE 1** Main Applications of HIS and Chemometrics in Foodstuff—Cont'd

Sample	Application	Analytical technique	Chemometrics technique	Reference
Strawberries	Estimation of physical and chemical properties	Vis–NIR HSI	PLS	[31]
	Prediction of the firmness	Vis–NIR HSI	MLR	[32]
	Detection of bruises	Vis–NIR HSI	ANN	[33]
Cherries	Discrimination between cherries with and without pits	Vis–NIR HSI	ANN	[34]
	Detection of pits	Vis–NIR HSI	PCA, ANN	
Mushrooms	Detection of bruises	Vis–NIR HSI	PCA	[35]
	Enzymatic browning	Vis–NIR HSI	PLS	[36]
	Early detection of freeze damage	Vis–NIR HSI	LDA	[37]
	Identify water matrix co-ordinates	NIR HSI	PLS	[38]
Peaches	Quantization of sugar content	NIR HSI	PLS	[39]
Pears	Detection of bruises	NIR HSI	MLC, EDC, MDC, SAM	[40]
Grapes	Quantization of anthocyanin	Vis–NIR HSI	Adaptive boosting, PLS	[41]
	Detection of canker lesions	Vis–NIR HSI	SID	[42]
Sample	Application	Analytical technique	Chemometrics technique	
Beef	Prediction of tenderness	Vis–NIR HSI	MLR, CDA, PLS	[43,44]
	Detection of bacterial spoilage	Vis–NIR HSI	MLR	[45]

Pork	Prediction of the quality grade	Vis–NIR HSI	ANN	[46,47]
	Detection of bacterial spoilage	Vis–NIR HSI	SVM	[45]
Chicken	Detection of skin tumours on chicken carcasses	Fluorescence HSI	FCM, ANN, SVM, PCA, DWT, KDA	[48–50]
	Detection of faecal contaminants	Vis–NIR HSI	PCA	[51–54]
Fish	Detection of parasites and blood spots on the surface	Vis–NIR HSI	PLS-DA, SIMCA	[55,56]
	Monitoring moisture distribution in dried salted fish	NIR HSI	PLS	[57]
	Prediction of water and fat content	NIR HSI	PLS	[58–60]
Sample	Application	Analytical technique	Chemometrics technique	
Cheese	Quantization of sugar, citric acid and salycilic acid in different cheeses	NIR HSI	PLS	[61,62]
	Classification of cheeses according to protein, fat and carbohydrate content	NIR HSI		
Grain	Classification and identification of grain specific classes	SWNIR HSI, NIR HSI and Vis–NIR HSI	PCA, PLS, LDA, ANN	[63–65]
	Prediction of chemical composition	NIR HSI	PLS	[66]
	Classification of grains according to hardness	Vis–NIR hyperspectral imaging	PCA, PLS-DA	[67]
	Detection of bacterial spoilage	Fluorescence HSI, NIR HSI	LDA, QDA, MDC	[64,68]

## 1.4 Objective of the Book Chapter

In this book chapter, we will not review the main applications of HSI and chemometrics for food quality assessment since this has already been extensively covered in several reviews [3,10] and the main applications have been highlighted in [Table 1](#). Instead, we will present a range of case studies showing the application and feasibility of the main chemometric techniques applied to different foodstuffs. Our objectives are to provide the reader with a detailed overview of how to apply the main chemometric techniques to HSI data, along with a critical discussion on their respective advantages and potential pitfalls. Although it is not possible to include examples for the myriad chemometric techniques available for data analysis, we aim to provide the reader with a selection that is useful and describe data analysis strategies that are transferable to other techniques. We will highlight the importance of unsupervised and supervised chemometric methods by giving full examples of the application of PCA, PLS-DA, and LDA in different situations as well as the use of PLS for quantitation purposes.

## 2 STRUCTURE OF A HYPERSPECTRAL IMAGE

There are three basic approaches for obtaining hyperspectral imaging data. Two configurations that imply the displacement of the sample (point and line scan settings, also known as whisker-broom and push-broom configurations), based on a step-and-acquire measuring mode, obtaining one single spectrum (point scan) or a line of spectra (line scan) of the surface in each movement; and the so-called plane scan system, which does not involve any moving part of the sample. Instead, light reflected from the whole surface of the sample is passed through specific filters ([Figure 3](#)).

The final result of the measurements with any of the three devices is a three-dimensional data structure or a hyperspectral data cube ('hypercube'). This structure can also be visualized as a three-dimensional array  $\mathbf{D}$  of dimensions  $(X \times Y \times \lambda)$  in which each pixel ( $x-y$  coordinate) is a spectrum of  $\lambda$  wavelengths ( $z$ -value) ([Figures 2 and 3](#)). There are differences in the quality of the collected data and the usefulness of each of the configurations must be considered beforehand [3,14]. For instance, when a more detailed structure is demanded, point scan configurations can be advised. However, the acquisition time of the full image in point scan mode is usually large ( $\sim 1$  h or more), so this method does not allow the real-time measurements required in process lines. In this case, line-scan or plane scan configurations can be recommended. In order to achieve high-quality hyperspectral imaging data, it is necessary to optimise the illumination system and acquisition parameters, such as integration time. In addition, each image must be calibrated. Detailed discussion of these issues is out of the scope of this book chapter, but can be found elsewhere [69,70].

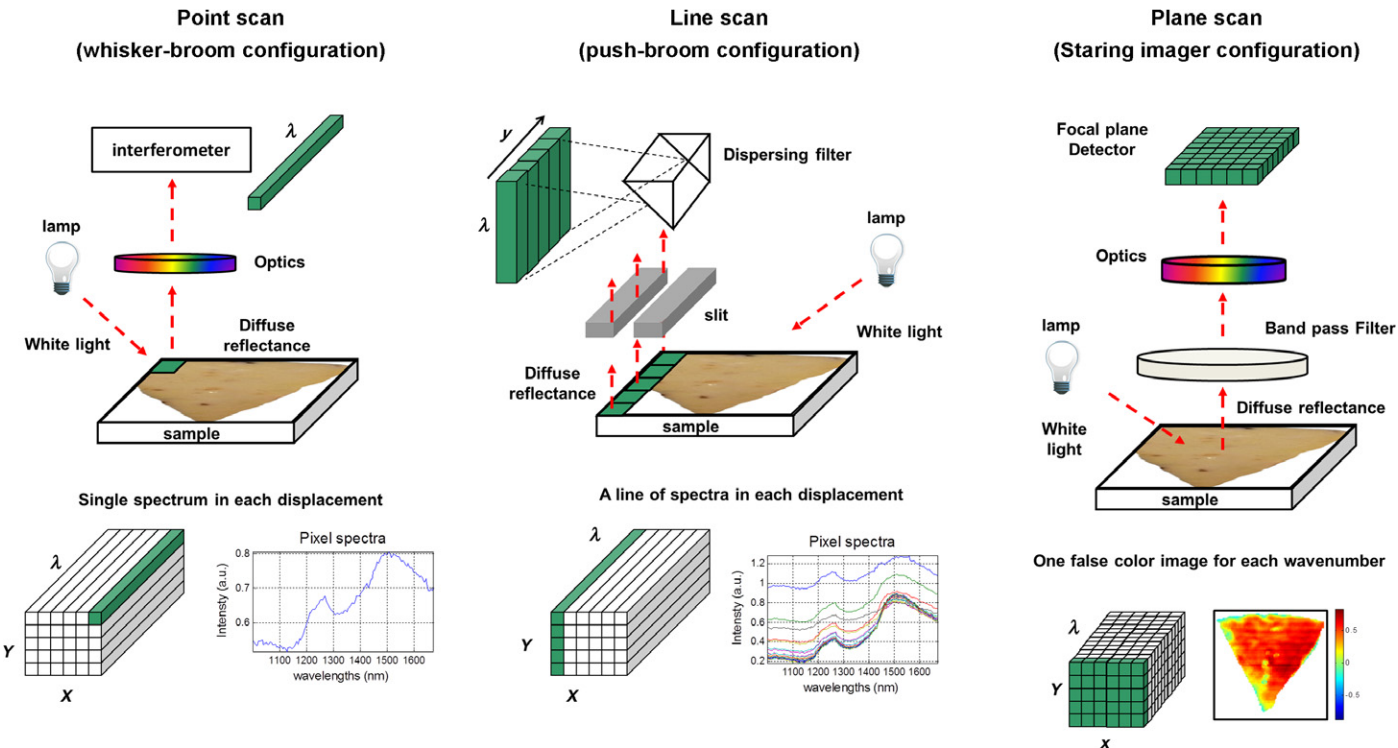


**FIGURE 3** Schematic representation of the three common configurations in hyperspectral imaging devices and structure of the final data cube of dimensions  $(X \times Y \times \lambda)$ . Slightly modified from [14] with permission of Springer.

### 3 HYPERSPECTRAL ANALYSIS AND CHEMOMETRICS: PRACTICAL EXAMPLES

#### 3.1 Overview of HSI Data Analysis

The final target of hyperspectral analysis is to correlate some feature of the individual objects in an image with some properties of interest. To achieve this target, multivariate data analysis is the key.

There are two main steps required in the analysis of hypercubes (Figure 4):

1. *Hypercube pre-processing*: Spatial and/or spectral pre-processing is mandatory to eliminate undesirable artefacts in the image (e.g. dead pixels, spiked wavelengths or undesired areas of the image) that can distort further multivariate models [71].
2. *Hypercube processing*: This stage is directly linked to the target pursued and refers to the application of multivariate models to the pre-processed hypercubes [2,14,15,71].

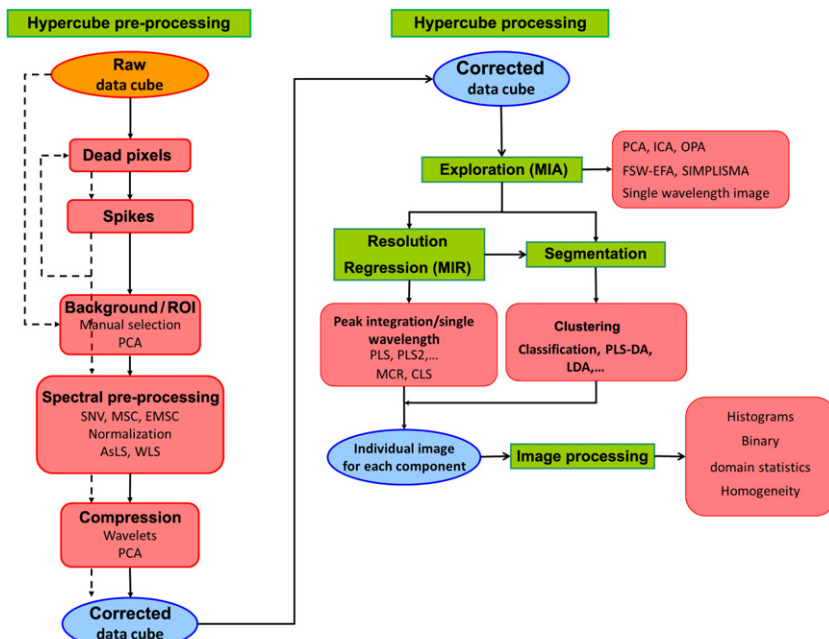


**FIGURE 4** Comprehensive flow-chart of the analysis of hypercubes. *Partially extracted and modified from [14,15,71].*

### 3.2 Pre-processing Methods

The target of spatial and spectral pre-processing is to avoid the influence of undesirable phenomena affecting the measurement, like areas of the scanned surface without interest (e.g. background), light scattering and shadows, particle size effects or detector artefacts. The main steps to prepare the hypercube for further data analysis can be summarized as follow [14]:

- *Image compression:* Hyperspectral images are usually composed of thousands or even millions of data points (e.g. one hyperspectral image of  $256 \times 256$  pixels operating at 150 wavebands contains more than 9 million data points). This amount of information requires much storage space, large transmission bandwidths, and long transmission times. Therefore, the compression of the image is sometimes very advantageous to retain only the needed information. Methods used to this respect are PCA, multivariate curve resolution (MCR), wavelets, or spatial binning. Also, the selection of informative wavelengths, directly linked to the property pursued may help for reducing the dimensionality of the data or even to promote faster identification of objects. As an example of this, [Figure 5](#) shows in the columns how different wavelengths give different information about a simple commercial cookie.
- *Region of interest (ROI) selection:* The geometry of the samples in the acquisition of the images plays an essential role in the selection of an ROI. Hyperspectral techniques usually acquire square images. If the sample does not cover all the scanned area, the area left outside the sample ('image background') must be eliminated, since this area is usually composed by highly noisy spectra. As an example, [Figure 5](#) shows the images at discrete wavelengths of one cookie. It can be observed that the background has a dark blue colour, denoting that this part of the image has been kept out of the analysis.
- *Dead pixels and spiked points/wavelengths:* Dead pixels are usually caused by anomalies in the detectors. Several methods have been proposed to detect and interpolate them, most of them reviewed by Vidal *et al.* [71]. They may be present as missing or zero values; and they can be one single pixel, entire lines of pixels, discrete wavelengths, or the whole spectral signal. Here we will not focus in talking about their detection and elimination, encouraging the readers to check the supplied references [71]. Nevertheless, it is important to highlight that these anomalies must be handled before the application of any other multivariate method, since they may easily distort further models.
- *Spectral pre-processing:* In the field of hyperspectral imaging, the most common practice is the adaptation of well-known pre-processing techniques of classical spectroscopy for spectral pre-processing [14,72]. Thus, de-noising, normalization, and derivatives are common practices for

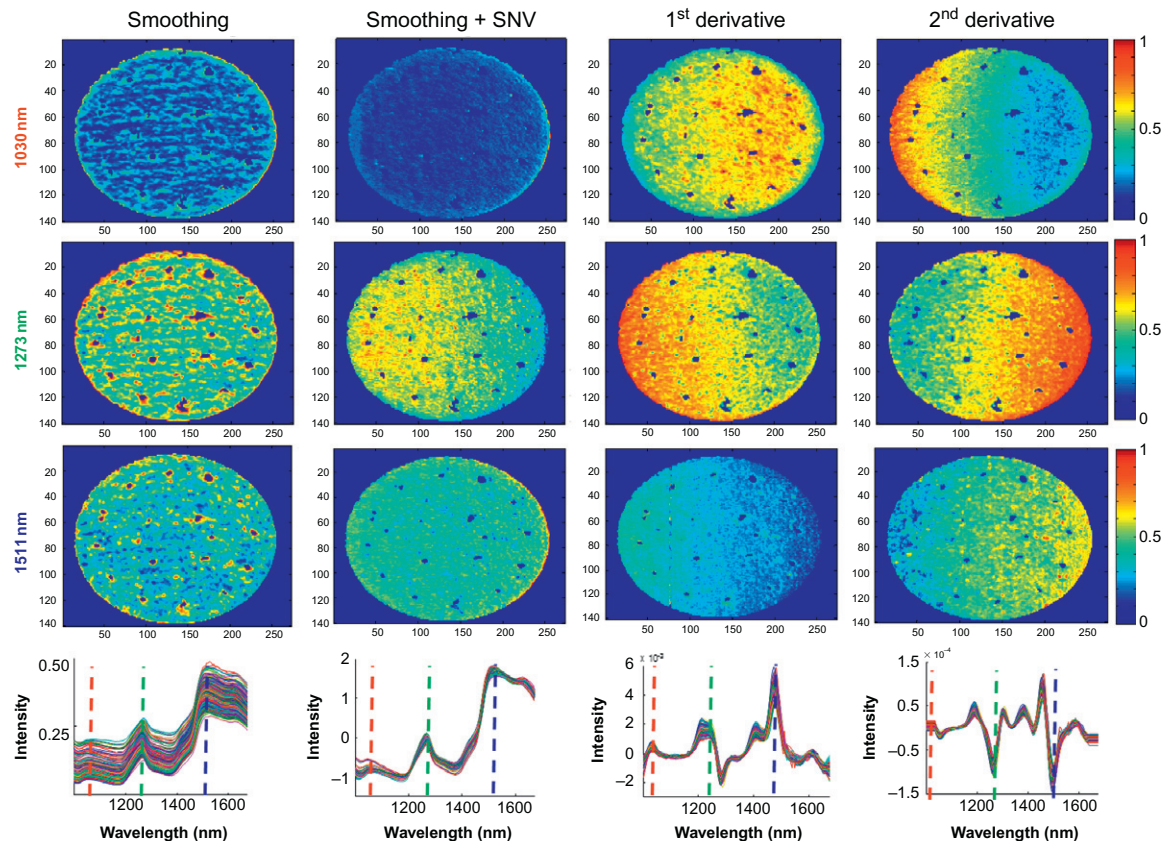


**FIGURE 5** Different spectral pre-processing methods and their influence in a commercial cookie.

suppressing scattering effects and undesirable spectral variability. Figure 5 shows the different information that can be highlighted when different pre-processing techniques are applied. For instance, at 1273 nm, smoothing basically eliminates the spectral noise, not correcting the scattering effect that is typical in NIR radiation. The effect of the scattering can be denoted at wavelengths 1273 and 1511 nm, where some effects of the roughness of the cookie can be observed. Once removing the scattering with, for instance standard normal variate (SNV), or after highlighting spectral features, with derivatives, other kinds of information can be extracted, such as an interesting profile in the second derivative mainly due to the lighting of the camera. As we will see in further sections, this lighting effect can be strongly minimized by using PCA. Thus, more chemical information can be obtained. Thus the application of the proper pre-processing methods helps to reduce spectral and spatial artefacts. Nevertheless, some pre-processing tools decrease the spatial resolution (e.g. binning techniques) or the spectral resolution (choosing the incorrect window size in the application of derivatives [72]). Therefore, the pre-processing step must be handled with care considering the spectral and the spatial variability, and, of course, the target pursued with the analysis.

### 3.3 Unsupervised Techniques to Explore the Image: PCA

PCA applied to HSI is, arguably, one of the most useful and widespread exploratory techniques within the framework of Food Science (see Table 1 for applications). Its ability to extract the main sources of variability and qualitatively study distribution of elements on a single image makes PCA a versatile and essential tool before applying any other multivariate model. PCA gives information about the main compounds (chemical compounds and physical artefacts) and their distribution in the measured surface.

The adaptation of the bilinear PCA model to hypercubes comes with a previous step of unfolding as indicated in Figure 6. Here, we can see that our dummy hyperspectral cube, denoted as  $\mathbf{D}(X,Y,\lambda)$  contains two main contributions (red and blue) with the peculiarity that the centre of the hypercube is a pixel containing both components. After unfolding (and thereby, obtaining the unfolded matrix  $\mathbf{D}(X^*Y,\lambda)$ ), PCA can be applied, decomposing the matrix into a score  $\mathbf{T}(X^*Y,F)$  and a loading  $\mathbf{P}^T(F,Y)$  matrix, depending on the number of principal components (PCs),  $F$ , with  $\mathbf{E}(X^*Y,\lambda)$  being the matrix containing the residuals.

The scores contain the concentration variability of the pixels, whereas the loadings contain the spectral variability. After application of PCA, the next step is the re-folding of the scores to obtain the so-called score images. In the case depicted in Figure 6, the two score images will contain the individual contribution for each component of the original hypercube, allowing the spatial visualization of the distribution of the components.

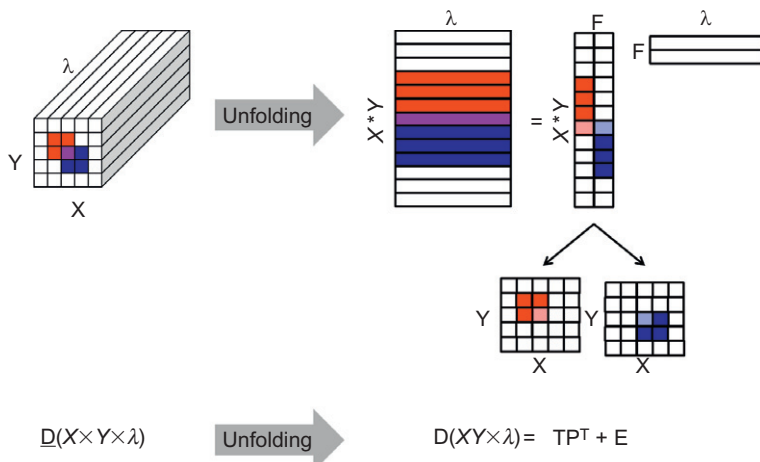


**FIGURE 6** Schematic representation of the adaptation and application of PCA to hypercubes. The figure shows a PCA model with two PCs, red and blue, having a pixel that is the mixture of both components.

One of the main drawbacks of PCA is that the spatial information is not taken into consideration when modelling. This has generated the adaptation of the general PCA method to methods more focussed on considering the spatial information gathered, by incorporating the spatial information in the analysis. For instance, methods like FSIW-EFA or enhancing contrast methods try to explore the analyzed surface merging surface and spectral information [73].

Despite the loss of the spatial information, PCA continues being a main tool in overviewing the main sources of variance in the hypercubes in both individual and set of samples. In individual samples, the target is the visualization of different elements within the surface; whereas the analysis of several samples together involves both the variance of the individual surfaces and also the variance between different samples. Two examples are shown herein: the first example shows the possibilities of finding water, fat, and protein sources in cheese. The image was acquired using a non-commercial NIR line mapping system from Foss (Foss A/S, Denmark) from which 16 spectra were collected in each acquisition from a linear detector array.

The second example classifies different types of almonds by using the information from their surfaces. The NIR image was acquired using a Sapphire Matrix NIR focal plane imaging system (Spectral Dimensions now Malvern Instruments Ltd, Malvern, Worcestershire, UK). The system comprised an NIR sensitive stirring-cooled InSb Focal Plane Array detector, four quartz-halogen lamps, which provided the illumination, and 2" polarization filters. The 81920 pixels ( $320 \times 256$  array) of the camera can be directed at fields of view varying from square millimetres to square inches.

### 3.3.1 Application 1: Detecting Water in Cheese in an Individual Sample

The PCA model of the cheese NIR picture of Figures 2 and 3 is depicted in Figure 7. The first three PCs explained more than 95% of the variance. As we can see in the figure, each one of the score maps is related to a different feature of the surface, since the colours of the maps relate to different parts of the cheese in the different PCs. Therefore, now the important step is to relate those changes with physico-chemical features of the sample. For doing that, the assignment of the main bands of the corresponding loading vectors must be done.

NIR spectroscopy is characterized by broad bands. Therefore, no strong assumptions must be done in the assignment of one PC to a particular component if there is no clear evidence of this. Nevertheless, following some of the typical wavebands indicated in references [74] it is possible to see that the first PC is mainly influenced by the water of the surface mainly located in the centre of the cheese, due to the nature of it. The second PC is highlighting the fat content in the edges of the surface and the third PC is more difficult to assign, being a combination of effects between fat and water.

This is an example of how PCA can highlight different features in the measured surfaces. As it was pointed out in Table 1 this is extremely useful in the detection of bruises, damages, contaminants, etc.

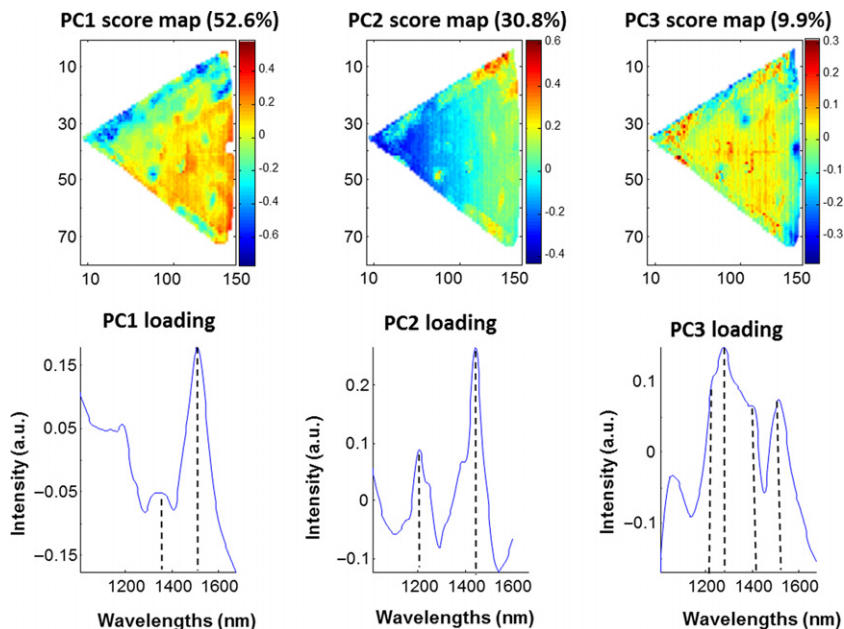


**FIGURE 7** PCA model of a slice of cheese. The score maps obtained for the first three PCs are depicted in the upper part; whereas the corresponding loadings are depicted in the bottom part.

### 3.3.2 Application 2: Unsupervised Classification of Almonds in a Set of Samples

Another of the main applications of PCA, as mentioned before, is for general study of the variability in many samples at the same time. With this, not only variability in the surface of the individual sample can be studied, but also the variability between different samples. An example of this is depicted in [Figure 8](#), where the hypercube of an image of eight almonds was analyzed by PCA. In the figure, the first row of almonds contains only sweet almonds; whereas the second row contains bitter almonds.

The data were previously pre-processed (smoothing with a window size of seven wavebands), SNV and mean centred. A PCA model with two PCs explained more than 95% of the variance, denoting the huge information contained in both. The score surfaces denoted a slight difference between sweet and bitter almonds. This difference can be checked with the loadings obtained of each PC. Nevertheless, the most informative plot is the projection of the PC1 versus PC2 scores, where the separation between the sweet and the bitter almonds is evident. This separation is given by a combination of PC1 and PC2. The great advantage of this is that now, the score surface obtained for PC2 can be directly related to this separation and, together with the loading for PC2, it can be possible to guess the chemical reason for this separation.

As we will see in [Section 3.4](#), this information can be used to construct further classification models and be able to discriminate between sweet and bitter almonds in a more robust manner. Nevertheless, PCA already gave us enough information to build more complex models.

## 3.4 Supervised Techniques for Classification of Features

Classification of features in hyperspectral imaging data is usually achieved by applying a classification method (e.g. LDA or PLS-DA) to a subset of spectral data from the hyperspectral image. Various methods exist to create calibration and validation datasets, which involve selecting spectra from a single or set of hyperspectral images. However, many supervised methods involve some work on the user's behalf, typically in selecting ROIs from imaging data that describe a particular object or material. The spectra contained in the ROIs are typically assigned a categorical variable according to their class membership. Spectra from a selection of ROIs can then be pooled in a two-dimensional matrix upon which a classification model is built. This model can then be applied to the individual spectra contained in the hyperspectral image to create a classification map. The extent of different features on the map can then be evaluated by counting the pixels in each class.

The general steps followed in the development and application of classification models with hyperspectral imaging data are shown in [Figure 9](#).

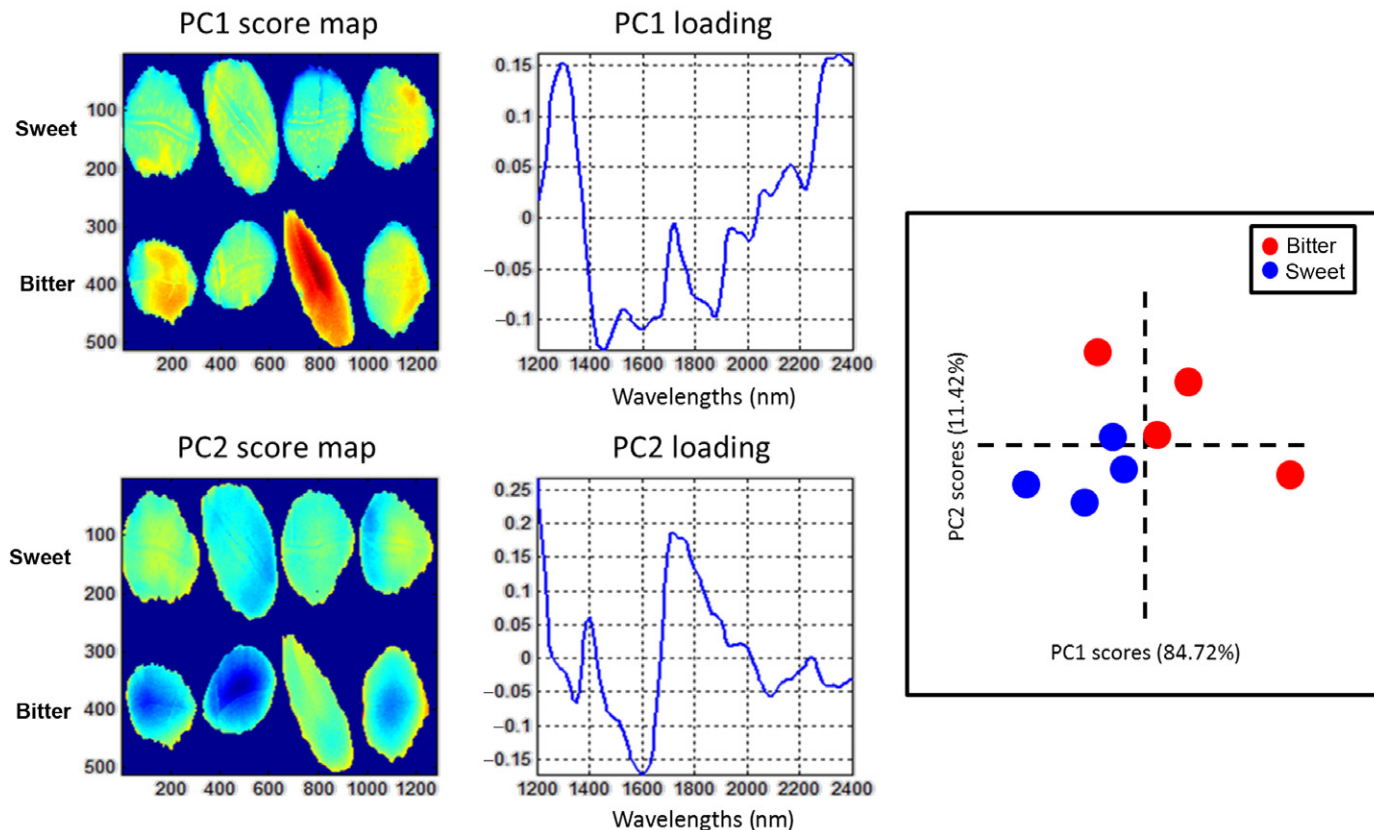


**FIGURE 8** Unsupervised classification of almonds by using PCA. The scores surfaces and the corresponding loadings are depicted in the left-most part; whereas the right-most part of the figure denotes the PC1 vs. PC2 plot of the mean spectrum for each almond. The colours of the score images are individually scaled in such a way that blue denotes intensity 0; whereas red denotes the maximum intensity 1.

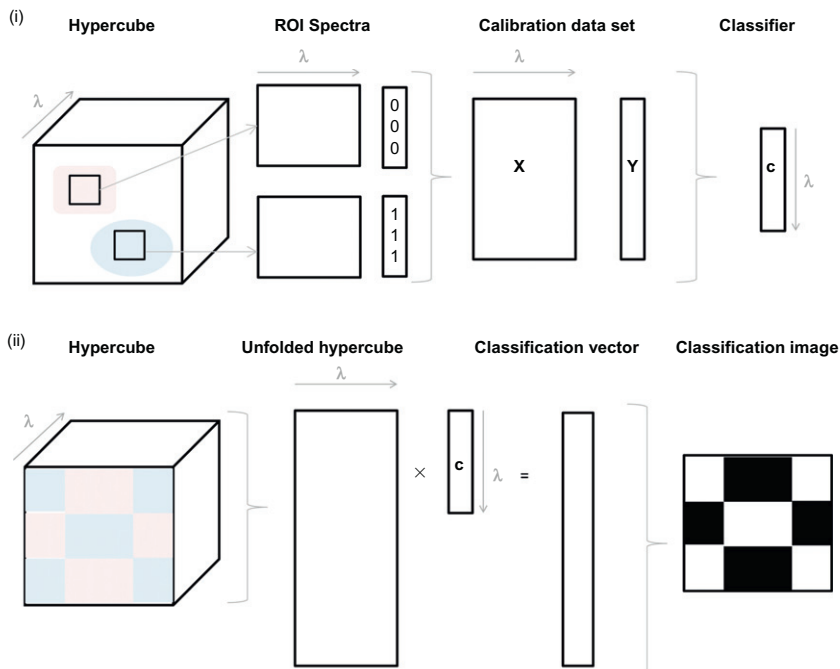


**FIGURE 9** General scheme for application of classification modelling to hyperspectral images ('hypercubes'). (i) selection of region of interest (ROI) spectra from sample images and construction of classifier (c), (ii) application of classifier to hypercube, resulting in classification image.

For brevity, the schematic shows two ROIs selected from a single image. However, in practice it is preferable to construct calibration datasets from multiple hyperspectral images, in order to span a greater variance.

### 3.4.1 Application: Detection of Contamination on Cheese Using LDA and PLS-DA

In this example, a slice of cheese with plastic contamination was imaged using the NIR HSI system described in [75]. An RGB image of the cheese and contamination is shown in Figure 10. The region imaged by the NIR HSI system is delineated by a red rectangle. A region of interest of approximately 80 pixels was selected from each object (i.e. plastic or cheese) for classification modelling. Plastic spectra were assigned a categorical variable of 1, while cheese spectra were assigned a value of 0. The mean spectrum of each object is also shown in Figure 10, top right. It is clear that the spectral profile of the contaminant is very different to that of the cheese sample, indicating that this will not be a difficult classification problem.

Fishers LDA finds an optimal linear projection that maximizes the between class variance while minimizing the within class variance. This is done by calculating Fishers linear discriminant. The original data are projected according to this transformation and classified according to their distance to each class (i.e. assigned to the class that they are closest to). Euclidean distance is typically used to measure the distance to class mean. In [Figure 10](#) (lower section), the results of applying Fishers LDA to the cheese/plastic dataset are shown. The LDA classifier works perfectly for discriminating between these two objects, due to the significant spectral

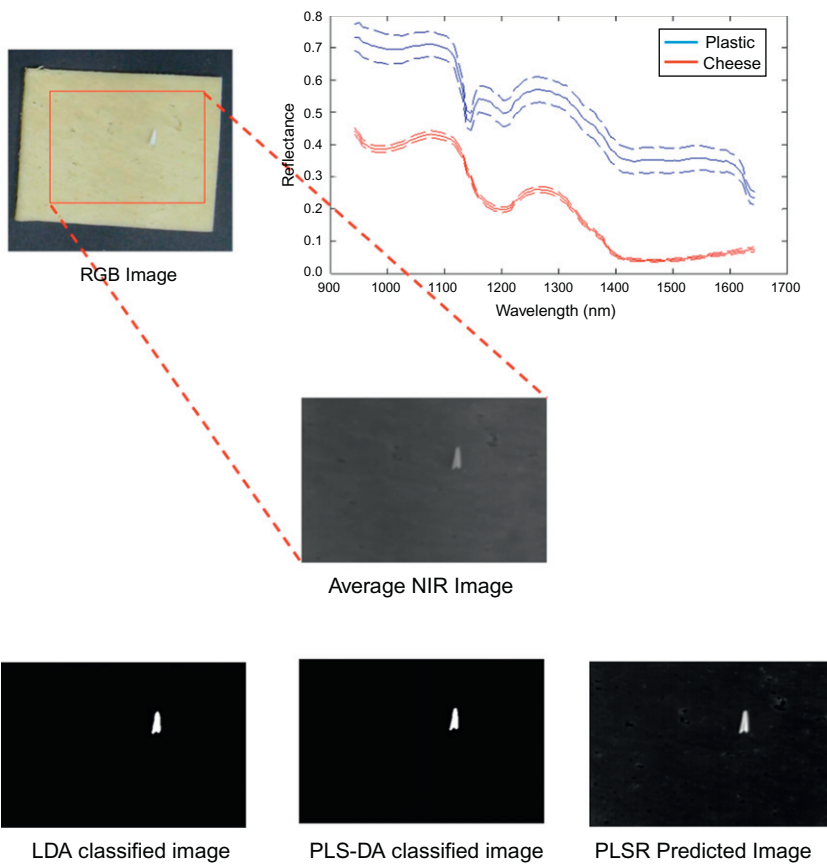


**FIGURE 10** Upper: RGB image of cheese sample with plastic contaminant. Average  $\pm$  standard deviation of ROI spectra for cheese and plastic are shown on the up right hand side of the upper portion of the figure. Middle: Average NIR hyperspectral image of the cheese/plastic dataset. Lower: results of building LDA and PLS-DA classifiers and applying it to the hypercube are shown. All of the pixels corresponding to the plastic contaminant are predicted as belonging to class '1' and all of the pixels corresponding to the cheese are predicted as belonging to class '0'. Also, the result of applying PLSR is shown, by applying a threshold of 0.5.

differences between them. Also shown in this figure is the mean NIR HSI image, from which the plastic is clearly identifiable as distinct from the cheese background. This is mainly due to differences in reflected light intensity from each object (the plastic reflects almost twice the amount of light that the cheese does, as can be seen in the spectra shown in [Figure 10](#)). The advantage of applying LDA in this case is that the classifier is based on the spectral profile of each class, rather than average light intensity, which could vary due to extraneous factors, such as sample height and morphology.

Application of PLS-DA differs somewhat to criterion based methods such as LDA. In this case, a PLS regression model is built to predict the categorical variable (0 and 1 in our case). The predicted values vary around 0 and 1. In order to turn this regression model into a discriminant model, it is necessary to choose a threshold, so that any predicted values above the threshold would be classified as belonging to class 1 (plastic) and all predicted values below the threshold would be classified as belonging to class 0 (cheese). It is common to apply a threshold value of 0.5 when the class values are in the [0,1] range and the number of spectra in each class is equal. However, when the number of spectra in each class is not the same, an alternate threshold may be required. This is usually selected by trial and error.

Application of the PLSR model to hypercube data results in a predicted image of spatially varying intensity for each class. However, thresholding this image so that all pixel values above 0.5 were classified as plastic and all pixel values less than 0.5 were classified as black results in a classification image identical to the LDA classification image ([Figure 10](#)).

In the example given here, the sample spectra were sufficiently different to allow classification by a relatively simple linear model (LDA). However, this type of modelling may not be successful if the sample spectra were more similar to each other. In addition, LDA does not perform well if the distribution of the data is non-normal. PLS-DA works slightly better in this situation, but generally kernel methods (e.g. Support Vector Machines) are necessary if the dataset is substantially nonlinear.

### 3.5 Regression Modelling for Obtaining Quantitative Information from Hyperspectral Images

Construction of regression models from hyperspectral imaging data differs from standard spectroscopic model development, where each spectrum ( $X_i$ ) has a corresponding measured variable ( $y_i$ ). Hyperspectral images typically contain thousands of spectra corresponding to the same measured variable. The standard approach to overcome this problem is to calculate a spectrum representing the sample. Commonly a mean or median spectrum is calculated from the spatial region of the sample that has been imaged. The mean spectra representing each sample in the calibration set are then pooled to form a matrix ( $\mathbf{X}$ ) and a regression method (e.g. PLSR) is applied to this matrix to

predict the corresponding measured (**Y**) values. Cross validation is usually applied for selection of model parameters (e.g. number of latent variables to include in a PLSR model). The resultant regression vector (**b**) can be applied to the unfolded original hyperspectral image, providing predictive values for each pixel in the image. Re-folding this image results in a prediction image. The steps involved in this process are summarized in [Figure 11](#) and exemplified in the following section.

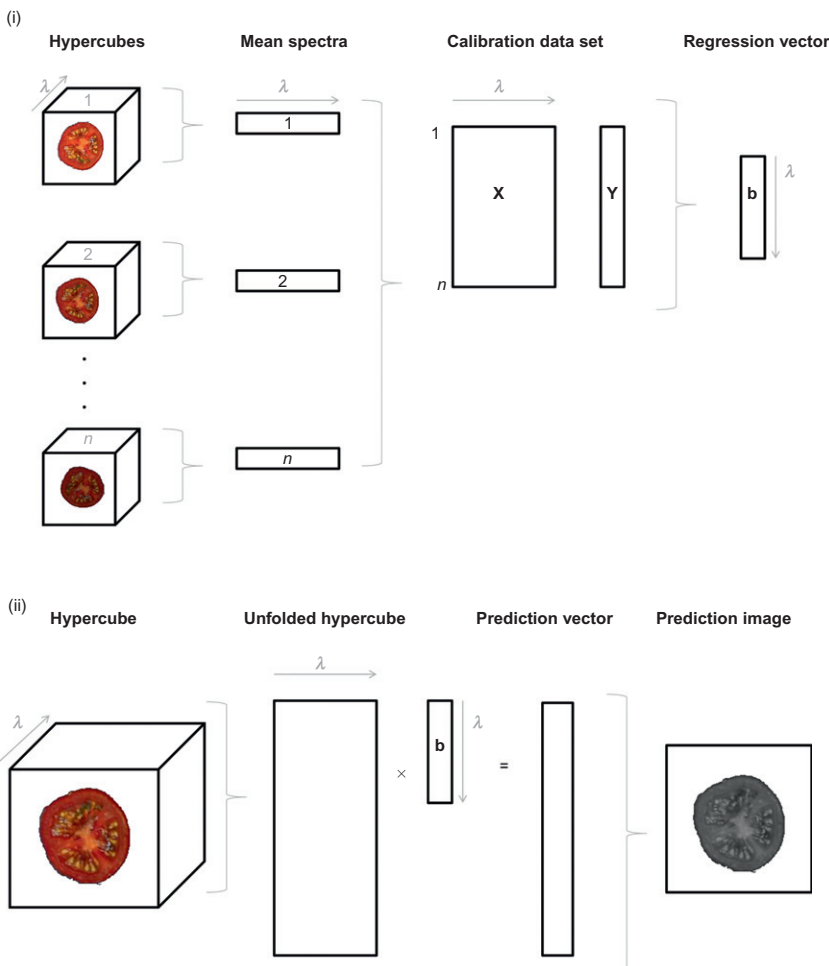


**FIGURE 11** Application of regression modelling to hyperspectral images ('hypercubes').  
 (i) selection of mean spectra from sample images and construction of regression vector (**b**),  
 (ii) application of regression model to hypercube, resulting in prediction image.

### 3.5.1 Application: PLS Regression for Evaluating Hydration of Chickpeas During Soaking

This dataset consisted of chickpeas (*Cicer arietinum L.*), hydrated to different moisture contents by immersion in tap water at  $40 \pm 1^\circ\text{C}$ . Ten chickpeas were removed from the water after the following soaking times: 30 min, 1, 2, 3, 4, 5, 6 h. Their surface was lightly dried using tissue paper and the samples were allowed to equilibrate with room temperature for 20 min. Each chickpea was subsequently sectioned along its central axis, and the inner surface of the chickpea was imaged using NIR hyperspectral imaging equipment described in [75]. The goal of this study was to use hyperspectral imaging to evaluate the internal distribution of moisture content in chickpeas at various stages during the process of soaking in water. Towards this aim, partial least squares regression models were constructed with the mean spectra of each chickpea, to predict moisture content.

On consideration of the prediction of moisture content over the chickpea surface (Figure 12) it is possible to appreciate the advantage of NIR hyperspectral imaging over conventional point spectroscopy. In the case where moisture content is low (during the first 2 h of soaking), the distribution of moisture content is not constant in the chickpea core. It is lowest at the centre of the chickpea because sufficient moisture has not yet reached this area at this early stage of the soaking process. As soaking proceeds, the distribution of water becomes more homogenous until 4–5 h soaking. These findings agree with previous research that measured the texture of chickpeas during the soaking process [76]. In that study, differences in texture were minimal after 4 h soaking at  $40^\circ\text{C}$ .

## 4 FINAL REMARKS

In the last few years, we experienced how the hyperspectral systems have been adapted from the remote sensing field to more dedicated applications

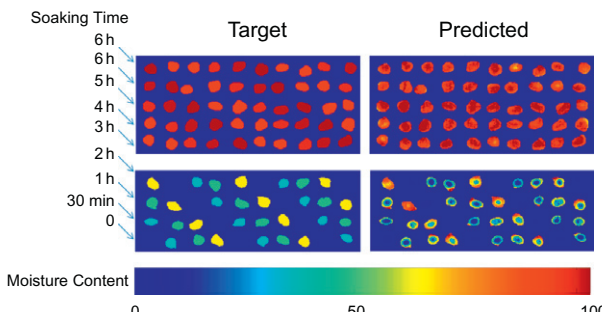


**FIGURE 12** Prediction images for moisture content in chickpeas during soaking. Target moisture contents are shown on left hand side and predicted moisture content is shown on the right hand side. Samples were arranged in a diagonal lattice according to soaking time, as shown in the target images.

in the laboratories or in the field, generating new devices and more interest in its application. This has been done thanks to the need of food scientist for fast, reliable and non-destructive analysis of food products. Even, the latest generation of HIS instrumentation enables acquisition of higher spectral and spatial resolution imagery thanks to the development of new and faster sensors.

We have also seen that hyperspectral imaging is inherently linked to multivariate data analysis. We count hundreds of algorithms that can be implemented/adapted to solve any question in HSI, and, the more important, powerful, and robust algorithms are continuously being improved in their adaptation to HIS requirements.

Throughout this book chapter, we have shown how hyperspectral devices and chemometric methods have been successfully implemented in many different areas of food sciences: From finding and detecting features in the surface of the samples, establishing classification models able to be installed in production lines for shortening purposes to quantification of features in the surface. Nevertheless, the binomial of HSI and chemometrics applied to food science is still, to some extent, in the growing phase. The application of more and more sophisticated algorithms to larger and larger image datasets in shorter time places a heavy demand on computer engines [11]. Much work remains to carefully construct software with intelligent implementations of algorithms to make proper use of this power.

## ACRONYMS

<b>ANN</b>	artificial neural networks—Unsupervised or supervised classification and quantization.
<b>AsLS</b>	assymmetric least squares—Spectral baseline correction
<b>CDA</b>	canonical discriminant analysis—Unsupervised pattern recognition
<b>CLS</b>	classical least squares—Quantization
<b>DWT</b>	discrete wavelet transformation—Spectral and/or spatial compression
<b>EDC</b>	Euclidean distance classification—Unsupervised classification
<b>EMSC</b>	extended multiplicative scatter correction—Spectral preprocessing (scattering minimization)
<b>FCM</b>	Fuzzy C-means—Unsupervised/supervised classification
<b>FDA</b>	food and drugs administration
<b>FSIW-EFA</b>	fixed size image window—evolving factor analysis—Surface screening for number of components
<b>GC-MS</b>	gas chromatography-mass spectrometry
<b>HPLC</b>	high performance liquid chromatography
<b>HSI</b>	hyperspectral imaging or hyperspectral image
<b>ICA</b>	independent component analysis—Unsupervised pattern recognition—Unsupervised classification

<b>k-NN</b>	k-nearest neighbour—Unsupervised classification
<b>KDA</b>	Kernel discriminant analysis—Unsupervised classification
<b>LDA</b>	linear discriminant analysis—Supervised classification
<b>MCR</b>	multivariate curve resolution—Curve resolution method
<b>MDC</b>	Mahalanobis distance classification—Unsupervised classification
<b>MIA</b>	multivariate image analysis—Unsupervised pattern recognition
<b>MLC</b>	maximum likelihood classification—Unsupervised classification
<b>MLR</b>	multilinear regression—Quantization
<b>MSC</b>	multiplicative scatter correction—Spectral pre-processing (scattering minimization)
<b>NIR</b>	near infrared
<b>OPA</b>	orthogonal projection approach—Unsupervised pattern recognition
<b>PAT</b>	process analytical technologies
<b>PCA</b>	principal component analysis—Unsupervised pattern recognition
<b>PLS/PLSR/</b>	partial least squares regression—Quantization
<b>PLS2</b>	
<b>PLS-DA</b>	partial least squares-discriminant analysis—Supervised classification
<b>QDA</b>	quadratic discriminant analysis—Supervised classification
<b>RGB</b>	red–green–blue colour space
<b>SAM</b>	spectral angle mapping—Unsupervised classification
<b>SID</b>	spectral information divergence—Unsupervised classification
<b>SIMCA</b>	soft independent modelling of class analogy—Supervised classification
<b>SIMPLISMA</b>	simple-to-use interactive self-modelling mixture analysis—Curve resolution method
<b>SNV</b>	standard normal variate—Spectral pre-processing (scattering minimization)
<b>SVM/SVMR</b>	support vectors machine—regression—Unsupervised pattern recognition, supervised classification, quantization
<b>WLS</b>	weighted least squares—Spectral baseline correction

## REFERENCES

- [1] Food, Drug Administration (FDA) . Guidance for industry. PAT—a framework for innovative pharmaceutical development, manufacturing, and quality assurance, 2004; <http://www.fda.gov/downloads/Drugs/Guidances/ucm070305.pdf>.
- [2] Gowen AA, Amigo JM. Applications of spectroscopy and chemical imaging in pharmaceutics. In: Popp J, Tuchin VV, Chiou A, Heinemann SH, editors. Handbook of biophotonics, volume 3: photonics in pharmaceutics, bioanalysis and environmental research. Berlin: Wiley; 2012.

- [3] Gowen AA, O'Donnell CP, Cullen PJ, Downey G, Frias JM. Hyperspectral imaging—an emerging process analytical tool for food quality and safety control. *Trends Food Sci Technol* 2007;18:590–8.
- [4] Amigo JM, Popielarz MJ, Callejon RM, Morales ML, Troncoso AM, Petersen MA, et al. Comprehensive analysis of chromatographic data by using PARAFAC2 and principal components analysis. *J Chromatogr A* 2010;1217:4422–9.
- [5] Garrido-Novell C, Pérez-Marin D, Amigo JM, Fernández-Novales J, Guerrero JE, Garrido-Varo A. Grading and color evolution of apples using RGB and hyperspectral imaging vision cameras. *J Food Eng* 2012;113:281–8.
- [6] Yu HL, MacGregor JF. Multivariate image analysis and regression for prediction of coating content and distribution in the production of snack foods. *Chemomet Intell Lab* 2003;67:125–44.
- [7] Lorente D, Aleixos N, Gomez-Sanchis J, Cubero S, Garcia-Navarrete OL, Blasco J. Recent advances and applications of hyperspectral imaging for fruit and vegetable quality assessment. *Food Bioprocess Technol* 2012;5:1121–42.
- [8] Elmasry G, Kamruzzaman M, Sun DW, Allen P. Principles and applications of hyperspectral imaging in quality evaluation of agro-food products: a review. *Crit Rev Food Sci Nutr* 2012;52:999–1023.
- [9] Feng YZ, Sun DW. Application of hyperspectral imaging in food safety inspection and control: a review. *Crit Rev Food Sci Nutr* 2012;52:1039–58.
- [10] Gowen A, Gaston E, Burger J. Hyperspectral imaging in process analytical technology for the food industry. Springer; 2012.
- [11] Burger J, Gowen A. Classification and prediction methods. In: Park B, editor. *Hyperspectral imaging technology in food and agriculture*. New York: Springer; 2012.
- [12] Gowen A, O'Donnell CP, O'Callaghan D, Burger J. Analytical methods: hyperspectral imaging for dairy products in encyclopedia of dairy science. In: Fuquay JW, editor. *Encyclopedia of dairy science*. Massachusetts: Elsevier; 2011.
- [13] Gowen A, Taghizadeh M, O'Donnell CP. Using hyperspectral imaging for quality evaluation of mushrooms. In: Da-Wen Sun, editor. *Hyperspectral imaging for food quality analysis and control*. Amsterdam: Elsevier; 2010.
- [14] Amigo JM. Practical issues of hyperspectral imaging analysis of solid dosage forms. *Anal Bioanal Chem* 2010;398:93–109.
- [15] Amigo JM, Cruz J, Bautista M, Maspoch S, Coello J, Blanco M. Study of pharmaceutical samples by NIR chemical-image and multivariate analysis. *Trac Trend Anal Chem* 2008;27:696–713.
- [16] Nicolai BM, Lotze E, Peirs A, Scheerlinck N, Theron KI. Non-destructive measurement of bitter pit in apple fruit using NIR hyperspectral imaging. *Postharvest Biol Technol* 2006;40:1–6.
- [17] Elmasry G, Wang N, Vigneault C. Detecting chilling injury in Red Delicious apple using hyperspectral imaging and neural networks. *Postharvest Biol Technol* 2009;52:1–8.
- [18] Noh HK, Lu RF. Hyperspectral laser-induced fluorescence imaging for assessing apple fruit quality. *Postharvest Biol Technol* 2007;43:193–201.
- [19] Mehl PM, Chen YR, Kim MS, Chan DE. Development of hyperspectral imaging technique for the detection of apple surface defects and contaminations. *J Food Eng* 2004;61:67–81.
- [20] Ariana D, Guyer DE, Shrestha B. Integrating multispectral reflectance and fluorescence imaging for defect detection on apples. *Comput Electron Agr* 2006;50:148–61.
- [21] Peirs A, Scheerlinck N, De Baerdemaeker J, Nicolai BM. Starch index determination of apple fruit by means of a hyperspectral near infrared reflectance imaging system. *J Near Infrared Spec* 2003;11:379–89.

- [22] Zhao JW, Vittayapadung S, Chen QS, Chaitep S, Chuaviroj R. Nondestructive measurement of sugar content of apple using hyperspectral imaging technique. *Maejo Int J Sci Technol* 2009;3:130–42.
- [23] Menesatti P, Zanella A, D'Andrea S, Costa C, Paglia G, Pallottino F. Supervised multivariate analysis of hyper-spectral NIR images to evaluate the starch index of apples. *Food Bio-process Technol* 2009;2:308–14.
- [24] Cheng X, Chen YR, Tao Y, Wang CY, Kim MS, Lefcourt AM. A novel integrated PCA and FLD method on hyperspectral image feature extraction for cucumber chilling damage inspection. *Trans ASAE* 2004;47:1313–20.
- [25] Liu Y, Chen YR, Wang CY, Chan DE, Kim MS. Development of hyperspectral imaging technique for the detection of chilling injury in cucumbers; Spectral and image analysis. *Appl Eng Agric* 2006;22:101–11.
- [26] Ariana DP, Lu RF, Guyer DE. Near-infrared hyperspectral. Reflectance imaging for detection of bruises on pickling cucumbers. *Comput Electron Agr* 2006;53:60–70.
- [27] Ariana DP, Lu RF. Evaluation of internal defect and surface color of whole pickles using hyperspectral imaging. *J Food Eng* 2010;96:583–90.
- [28] Blasco J, Aleixos N, Gomez J, Molto E. Citrus sorting by identification of the most common defects using multispectral computer vision. *J Food Eng* 2007;83:384–93.
- [29] Gomez-Sanchis J, Gomez-Chova L, Aleixos N, Camps-Valls G, Montesinos-Herrero C, Molto E, et al. Hyperspectral system for early detection of rottenness caused by *Penicillium digitatum* in mandarins. *J Food Eng* 2008;89:80–6.
- [30] Li JB, Rao XQ, Ying YB. Detection of common defects on oranges using hyperspectral reflectance imaging. *Comput Electron Agr* 2011;78:38–48.
- [31] Elmasry G, Wang N, ElSayed A, Ngadi M. Hyperspectral imaging for nondestructive determination of some quality attributes for strawberry. *J Food Eng* 2007;81:98–107.
- [32] Lu RF, Peng YK. Hyperspectral scattering for assessing peach fruit firmness. *Biosyst Eng* 2006;93:161–71.
- [33] Nagata M, Tallada JG, Kobayashi T. Bruise detection using NIR hyperspectral imaging for strawberry (*Fragaria x ananassa* Duch.). *Environ Control Biol* 2006;44:133–42.
- [34] Qin J, Lu R. Detection of pits in tart cherries by hyperspectral transmission imaging. *Trans ASAE* 2005;48:1963–70.
- [35] Gowen AA, O'Donnell CP, Taghizadeh M, Cullen PJ, Frias JM, Downey G. Hyperspectral imaging combined with principal component analysis for bruise damage detection on white mushrooms (*Agaricus bisporus*). *J Chemometr* 2008;22:259–67.
- [36] Taghizadeh M, Gowen AA, O'Donnell CP. Comparison of hyperspectral imaging with conventional RGB imaging for quality evaluation of *Agaricus bisporus* mushrooms. *Biosyst Eng* 2011;108:191–4.
- [37] Gowen AA, Taghizadeh M, O'Donnell CP. Identification of mushrooms subjected to freeze damage using hyperspectral imaging. *J Food Eng* 2009;93:7–12.
- [38] Gowen AA, Tsenkova R, Esquerre C, Downey G, O'Donnell CP. Use of near infrared hyperspectral imaging to identify water matrix co-ordinates in mushrooms (*Agaricus bisporus*) subjected to mechanical vibration. *J Near Infrared Spec* 2009;17:363–71.
- [39] Guo F, Cao Q, Nagata M, Tallada JG. Nir hyperspectral imaging measurement of sugar content in peach using PLS regression. *J Shanghai Jiao Tong Univ (Sci)* 2007;12:597–601.
- [40] Zhao JW, Ouyang Q, Chen QS, Wang JH. Detection of bruise on pear by hyperspectral imaging sensor with different classification algorithms. *Sensor Lett* 2010;8:570–6.
- [41] Fernandes AM, Oliveira P, Moura JP, Oliveira AA, Falco V, Correia MJ, et al. Determination of anthocyanin concentration in whole grape skins using hyperspectral imaging and adaptive boosting neural networks. *J Food Eng* 2011;105:216–26.

- [42] Qin JW, Burks TF, Ritenour MA, Bonn WG. Detection of citrus canker using hyperspectral reflectance imaging with spectral information divergence. *J Food Eng* 2009;93:183–91.
- [43] Cluff K, Naganathan GK, Subbiah J, Lu R, Calkins CR, Samal A. Optical scattering in beef steak to predict tenderness using hyperspectral imaging in the VIS-NIR region. *Sens Instrum Food Qual* 2008;2:189–96.
- [44] Naganathan GK, Grimes LM, Subbiah J, Calkins CR, Samal A, Meyer GE. Visible/near-infrared hyperspectral imaging for beef tenderness prediction. *Comput Electron Agr* 2008;64:225–33.
- [45] Peng YK, Zhang J, Wang W, Li YY, Wu JH, Huang H, et al. Potential prediction of the microbial spoilage of beef using spatially resolved hyperspectral scattering profiles. *J Food Eng* 2011;102:163–9.
- [46] Qiao J, Ngadi MO, Wang N, Gariepy C, Prasher SO. Pork quality and marbling level assessment using a hyperspectral imaging system. *J Food Eng* 2007;83:10–6.
- [47] Qiao J, Wang N, Ngadi MO, Gunenc A, Monroy M, Gariepy C, et al. Prediction of drip-loss, pH, and color for pork using a hyperspectral imaging technique. *Meat Sci* 2007;76:1–8.
- [48] Kim I, Xu CZ, Kim MS. Poultry skin tumor detection in hyperspectral images using radial basis probabilistic neural network. In: Advances in neural networks—ISNN 2006, Pt 3, Proceedings, vol. 3973. 2006. p. 770–6.
- [49] Kim I, Kim MS, Chen YR, Kong SG. Detection of skin tumors on chicken carcasses using hyperspectral fluorescence imaging. *Trans ASAE* 2004;47:1785–92.
- [50] Xu C, Kim I, Kim MS. Poultry skin tumor detection in hyperspectral reflectance images by combining classifiers; Image analysis and recognition, lecture note in computer science. In: Image analysis and recognition, 4th International Conference, ICIAR 2007. Montreal: Springer; 2007. p. 1289–96.
- [51] Park B, Lawrence KC, Windham WR, Buhr RJ. Hyperspectral imaging for detecting fecal and ingesta contaminants on poultry carcasses. *Trans ASAE* 2002;45:2017–26.
- [52] Park B, Lawrence KC, Windham WR, Smith DP. Performance of hyperspectral imaging system for poultry surface fecal contaminant detection. *J Food Eng* 2006;75:340–8.
- [53] Heitschmidt GW, Park B, Lawrence KC, Windham WR, Smith DP. Improved hyperspectral imaging system for fecal detection on poultry carcasses. *Trans ASABE* 2007;50:1427–32.
- [54] Lawrence KC, Windham WR, Park B, Smith DP, Poole GH. Comparison between visible/NIR spectroscopy and hyperspectral imaging for detecting surface contaminants on poultry carcasses. *Proc SPIE* 2004;5271:35–42.
- [55] Heia K, Sivertsen AH, Stormo SK, Ellevoll E, Wold JP, Nilsen H. Detection of nematodes in cod (*Gadus morhua*) fillets by imaging spectroscopy. *J Food Sci* 2007;72:E11–E15.
- [56] Wold JP, Westad F, Heia K. Detection of parasites in cod fillets by using SIMCA classification in multispectral images in the visible and NIR region. *Appl Spectrosc* 2001;55:1025–34.
- [57] Wold JP, Johansen IR, Haugholt KH, Tschudi J, Thielemann J, Segtnan VH, et al. Non-contact transfectance near infrared imaging for representative on-line sampling of dried salted coalfish (bacalao). *J Near Infrared Spec* 2006;14:59–66.
- [58] Elmasy G, Wold JP. High-speed assessment of fat and water content distribution in fish fillets using online imaging spectroscopy. *J Agric Food Chem* 2008;56:7672–7.
- [59] Segtnan VH, Hoy M, Sorheim O, Kohler A, Lundby F, Wold JP, et al. Noncontact salt and fat distributional analysis in salted and smoked salmon fillets using X-ray computed tomography and NIR interactance imaging. *J Agric Food Chem* 2009;57:1705–10.
- [60] Segtnan VH, Hoy M, Lundby F, Narurn B, Wold JP. Fat distribution analysis in salmon fillets using non-contact near infrared interactance imaging: a sampling and calibration strategy. *J Near Infrared Spec* 2009;17:247–53.

- [61] Burger J, Geladi P. Hyperspectral NIR image regression part II: dataset preprocessing diagnostics. *J Chemometr* 2006;20:106–19.
- [62] Burger J, Geladi P. Hyperspectral NIR imaging for calibration and prediction: a comparison between image and spectrometer data for studying organic and biological samples. *Analyst* 2006;131:1152–60.
- [63] Mahesh S, Manickavasagan A, Jayas DS, Paliwal J, White NDG. Feasibility of near-infrared hyperspectral imaging to differentiate Canadian wheat classes. *Biosyst Eng* 2008;101:50–7.
- [64] Singh CB, Jayas DS, Paliwal J, White NDG. Detection of insect-damaged wheat kernels using near-infrared hyperspectral imaging. *J Stored Prod Res* 2009;45:151–8.
- [65] Wallaya C, Missotten B, De Baerdemaeker J, Saeys W. Hyperspectral waveband selection for on-line measurement of grain cleanliness. *Biosyst Eng* 2009;104:7.
- [66] Weinstock BA, Janni J, Hagen L, Wright S. Prediction of oil and oleic acid concentrations in individual corn (*Zea mays* L.) kernels using near-infrared reflectance hyperspectral imaging and multivariate analysis. *Appl Spectrosc* 2006;60:9–16.
- [67] Williams P, Geladi P, Fox G, Manley M. Maize kernel hardness classification by near infrared (NIR) hyperspectral imaging and multivariate data analysis. *Anal Chim Acta* 2009;653:121–30.
- [68] Singh CB, Jayas DS, Paliwal J, White NDG. Detection of midge-damaged wheat kernels using short-wave near-infrared hyperspectral and digital colour imaging. *Biosyst Eng* 2010;105:380–7.
- [69] Geladi P, Burger J, Lestander T. Hyperspectral imaging: calibration problems and solutions. *Chemometr Intell Lab* 2004;72:209–17.
- [70] Boldrini B, Kessler W, Rebnera K, Kessler R. Hyperspectral imaging: a review of best practice, performance and pitfalls for inline and online applications. *J Near Infrared Spec* 2012;20:438–508.
- [71] Vidal M, Amigo JM. Pre-processing of hyperspectral images. Essential steps before image analysis. *Chemometr Intell Lab* 2012;117:138–48.
- [72] Rinnan A, van den Berg F, Engelsen SB. Review of the most common pre-processing techniques for near-infrared spectra. *Trac Trend Anal Chem* 2009;28:1201–22.
- [73] de Juan A, Maeder M, Hancewicz T, Tauler R. Local rank analysis for exploratory spectroscopic image analysis. Fixed size image window-evolving factor analysis. *Chemometr Intell Lab* 2005;77:64–74.
- [74] Sasic S, Ozaki Y. Band assignment of near-infrared spectra of milk by use of partial least-squares regression. *Appl Spectrosc* 2000;54:1327–38.
- [75] Esquerre C, Gowen A, Burger J, Downey G, O'Donnell CP. Suppressing sample morphology effects in near infrared spectral imaging using chemometric data pre-treatments. *Chemometr Intel Lab* 2012;117:129–37.
- [76] Gowen A, Abu-Ghannam N, Frias J, Oliveira J. Modelling the water absorption process in chickpeas (*Cicer arietinum* L.)—the effect of blanching pre-treatment on water intake and texture kinetics. *J Food Eng* 2007;78:810–9.